Fingerprint Liveness Detection using Multi-Orthant Coding

Feng Wang, Jian Cheng, and Hongsheng Li

***Abstract*—Attacking fingerprint-based biometric systems by presenting fake fingers is a serious threat for unattended devices. In this paper, a simple but effective software-based approach is proposed to defend the fake finger's attack. We segment the local texture feature space into multiple orthants by their PCA hyperplanes. Through a specific coding algorithm, the segmentation task can be performed with a small number of convolutions. In this framework, the accuracy increases with the dimension of the feature. Because of the high efficiency of our algorithm, it is very convenient to generate a very high dimensional feature. The experimental results show that our algorithm remarkably outperforms the state-of-the-art approaches in the Liveness Detection Competition 2011 (LivDet2011) benchmark.**

***Index Terms*—fingerprint liveness detection, Multi-Orthant Coding, high dimensional feature**

I. Introduction

In recent years, fingerprint verification systems for personal identity recognition reached a high degree of accuracy. Unfortunately, various of fake fingerprint molds has been developed to attack the biometric authentication system [1]. Fake Fingers made by Play-Doh, gelatin, latex, wood glue, and even the printed paper can pass some authentication systems. From a security perspective, fingerprint authentication systems should have the ability to distinguish authentic or fake finger samples. This requirement motivates researchers to find effective methods to discriminate fake fingers from real ones.

A. Related Works

To solve the issue, one intuitive approach is to add more sensors to the hardware of authentication system, such as temperature, pulse oximetry, blood flow, electrical characteristics [2], spectral characteristics [3], odor [4], heartbeat [5]. These devices are more usually expensive as they require additional hardware and may be not convenient to the users. For example, one commercially fingerprint verification system with spoof detection is from Lumidigm using a multi-spectral sensor: spectral qualities of live skin, chromatic texture of skin, subsurface image of live skin, and blanching on contact [6]. This method requires to purchase a specific scanners which are not applicable to other optical fingerprint sensors. Moreover, hardware systems may also be cheated unless they keep up with the hackers' new techniques.

These situations impel researchers to develop software-based approaches, since they do not require additional hardware, and they work with the images captured by existing sensors. Most existing fingerprint identify systems can easily adopt these software-based approaches by updating the embedded software. When a new hacking technique appears, the systems can be updated to discriminate new types of fake fingers in a short time.

The software-based techniques are divided into two catogories by their input data: dynamic frame sequences based methods and static images based methods. Dynamic techniques, such as skin deformation based ones [7], [8] and elasticity patterns based ones [9], [10], extract features from a series frames collected by sensors. The skin deformation approaches [7], [8], requires the users to press on the sensor by different pressure and rotate the pressure center. Since the fake fingers made by rigid materials usually have less distortion than the live ones, they designed various algorithms to analyse the distortion. The elasticity-based approaches [9], [10] are similar, utilizing the stereo shape and the elasticity of real finger. In the initial frames, real fingers only have small region touched on finger sensor, while the flat fake fingers fully cover the sensor and their images have no difference with later frames.

Static images based approaches utilizes less information compared with dynamic ones. Up to now, no obviously physical feature has been found to provide a clear standard of judging the liveness of fingerprint. Some researchers did preliminary analyses in using statistical patterns, such as power spectrum [11], wavelet [12], [13], [14], curvelet [15] and fusion of multiple static feature [16]. Perspiration pattern and other noise in valley of fingers are widely considered to be discriminative [17], [18], [19]. However, whether perspiration exists or not is determined by the users, not the authentication systems. Pores on the ridge are also an extensively used pattern [16], [19], because the abraded fake fingers would not contain the tiny details.

To get rid of the affection of various fingerprint curve directions, some reseachers extract features along the fingerprint curves to achieve rotation-invariance. Derakhshani et al. [17], and Choi et al. [16] use a 1-D long signal on the ridges, and find that the 11 to 33 FFT points have considerable ability of discrimination. Tan et al. [19] add signal samples from valleys, which denotes the perspiration and noise. Because they intent to avoid the influence of the width, only the thinned skeletons of ridges and valleys are utilized, and leave the rest information from slopes apart.

Thanks to the Liveness Detection Competition [20], the techniques of fingerprint liveness detection boom in recent years. More researchers join in this area and various texture analyse methods have been applied on the LivDet09 [21],

F. Wang is with the Department of Electronic Engineering, University of Electronic Science and Technology of China, Chengdu, Sichuan, 611731 China e-mail: feng.wff@gmail.com .

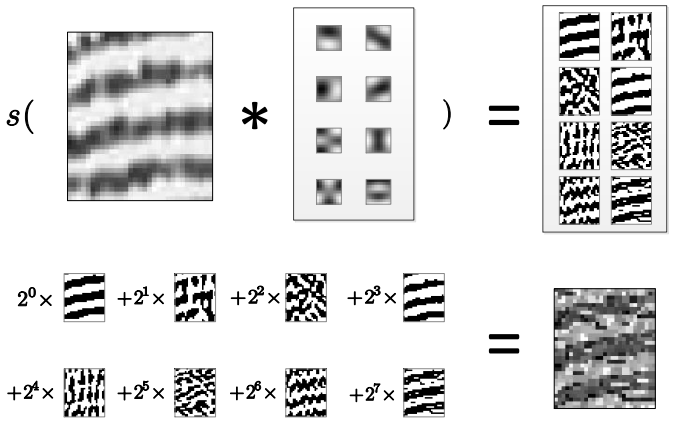

Fig. 1. The procedure of the *MOC* pipeline. The feature is represented as the histogram of the image at bottom right. The $s(x)$ is defined in Equation (2).

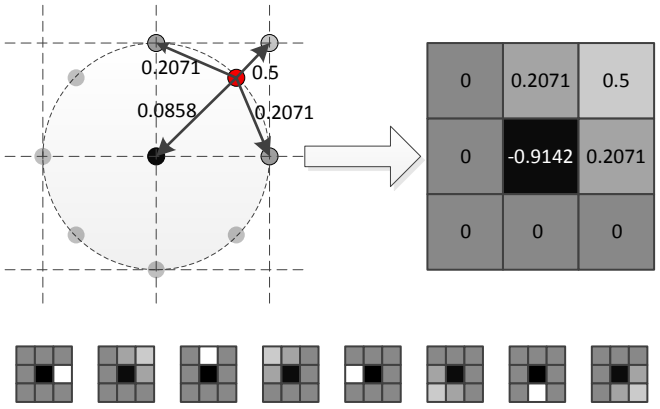

Fig. 2. Top: the bi-linear interpolation for the calculation of the filters in $LBP_{8,1}$. Bottom: the filter bank of $LBP_{8,1}$.

LivDet11 [20], and LivDet13 [22]. Local binary pattern (LBP) [23] and local phase quantization (LPQ) [24] have shown outstanding ability of discrimination [25]. The two feature descriptors have a framework, which consists of local 2D filtering, feature binarization, and the arrangement of the binary features. Different improvements are proposed for both LBP and LPQ features. For instance, Jia et al. [26] combined the LBP features from multiple scales (MSLBP) to obtain more information, and Ghiani et al. [27] proposed a method to learn a new filter bank from natural images (BSIF) by Independent Component Analysis (ICA).

B. Contribution

Our main contribution lies in three aspects. First, we have found that all the state-of-the-art algorithms share the same coding scheme, which is named as *Multi-Orthant Coding (MOC)* by us (Section II). With the *MOC* scheme, even random parameters could lead to a satisfying accuracy. Second, we analyse the property of *MOC* and propose to use Principle Component Analyse (PCA) to learn filter banks for it (Section III). Last, we proposed a series of techniques to promote the performance of the *MOC*, such as high dimensional strategy (Section IV), background filtering (Section V-C) and normalization (Section V-D).

Moreover, we have discovered the non-ignorable role of the background in fingerprint images. They also provide important information for discriminating fake fingerprints from live ones. The explanation and experiment details are described in Section V-C.

II. Multi-Orthant Coding (MOC)

Some of the previous algorithms, such as LBP [28] and its extensions [23], [26], LPQ [24] and BSIF [27], share a same coding scheme, and we call it *Multi-Orthant Coding (MOC)*.

A. Coding Procedure

For a given filter bank that contains d filters f_i $(i = 1 \cdots d)$ with window size of $s \times s$, the *MOC* code $C(\mathbf{I})$ of a given image $\mathbf{I}$ is calculated as

$$C(\mathbf{I}) = \sum_{i=1}^{d} 2^i \cdot s(\mathbf{I} * f_i) \tag{1}$$

where,

$$s(x) = \begin{cases} 1 & if\ x \geq 0 \\ 0 & if\ x < 0 \end{cases} \tag{2}$$

and the symbol $*$ denotes the convolution operator.

The most common feature of *MOC* is the histogram of $C(\mathbf{I})$. Since the codes in $C(\mathbf{I})$ vary from 0 to $2^d - 1$, the histogram features have totally 2^d dimensions. The whole coding procedure of *MOC* is shown with our learned filter bank in Fig. 1.

B. Local Binary Pattern and Its Extend Versions

The original LBP (*OLBP*) operator was first proposed by Ojala et al. [28]. It is well-known for its perfect performance in illumination and rotation variant texture analysis. However, the rotation-invariant version of LBP is inadequate to the minutia classification task as experimental results [26] shown. In this paper, we stop attempting to perform any rotation invariance as well.

Since it is a fundamental algorithm in computer vision, too many papers have described the mathematics procedure of it. Here we will explain the algorithm from a new perspective of filter bank. The filter bank of *OLBP* contains 8 filters with size of 3×3 (Fig. 3), which are used to calculate the gradient of the image in 8 different directions. The following steps are just the same as the *MOC*. Finally, 256-dimensional histogram features are extracted to describe the texture of images.

The *OLBP* is extended to different radius and various amount of sampling points in [23], which is referred to as $LBP_{P,R}$. Different from the *OLBP*, $LBP_{P,R}$ is no longer calculated on the integral grid positions. Instead, they are computed on specified shapes such as circle or ellipse, which means the signals are sampled at some floating points (Fig. 2 top left). The most widely used sampling strategy of $LBP_{P,R}$ is bi-linear interpolation, which can be expressed as a linear combination of the neighbourhood integral points around the

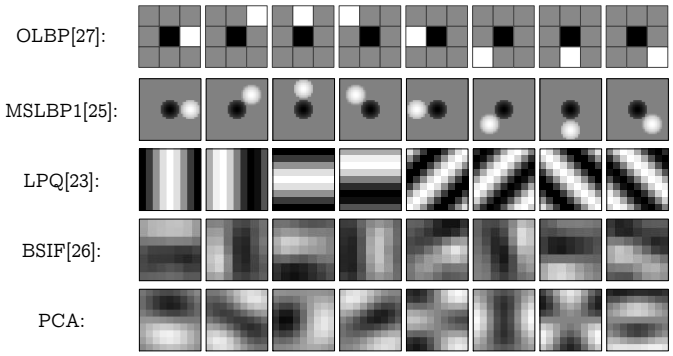

Fig. 3. Four different filter banks in the corresponding algorithms, where OLBP is short for the original LBP [28]. Filters of MSLBP2 is not listed here because they are just enlarged ones of the original LBP. The filters of BSIF in this figure are a little different from the ones in [27] because we calculate them with different natural images.

sampling points (Fig. 2 top left). The sampling procedure is equivalent to a group of well-designed filters shown in Fig. 2 top right. Thus, the $LBP_{P,R}$ can also be concluded as a special case of the *MOC*. By replacing the filters in the *MOC* with the ones illustrated in Fig. 2 bottom, we will get the feature histogram of $LBP_{P,R}$ in the same framework.

C. The Filter Banks of LPQ and BSIF

The Local Phase Quantization (LPQ) [24] is a blur-invariant texture classification method. It is able to represent all spectrum characteristics of images in a very compact feature representation. The eight filters are generated by short term Fourier transform (STFT) in four directions and two phases.

Binarized statistical image feature (BSIF) [27] learns filters from natural images using independent component analysis (ICA). The size and number of the filters can be selected manually. The authors suggested to choose 12 filters with window size of 7×7 to get a better performance.

The following steps of LPQ and BSIF are also the same as *MOC*. The filters employed by original LBP [28], $\text{LBP}_{8,1}$ [23], MSLBP [26], LPQ [24] and BSIF [27] are illustrated with ours (PCA) in Fig. 3. Since the only difference of these algorithms is the design of the filter banks, we regard these algorithms as special cases of *MOC*.

D. Geometric Perspective

Note that the hyperplanes $\mathbf{f}_i^T\mathbf{x} = 0$ $(i = 1 \cdots d)$ cut the $\mathbb{R}^{s^2}$ into 2^d orthants (Fig. 4 left), where the bold $\mathbf{f}_i$ denotes the i-th **vectorized** filter. Each code in $C(\mathbf{I})$ ranges from 0 to 2^d, which is the serial number of the orthant that the corresponding local image patch vector lies in. Simultaneously, each value in the histogram feature denotes how many patch vectors are located in each orthant (Fig. 4 right). This is why we name the coding scheme as *Multi-Orthant Coding (MOC)*.

However, even though we call it "orthant", the hyperplanes need not to be strictly orthogonal with each other. For instance, the filter banks of LBP and its extended versions are non-orthogonal, and this is main reason why the histogram of LBP is always unbalanced and redundancy (Fig. 4).

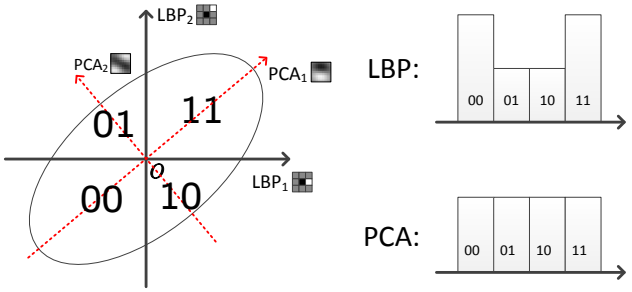

Fig. 4. Geometric explanation of *Multi-Orthant Coding (MOC)* scheme in $\mathbb{R}^2$. Note that the histogram of LBP [28] is not balance, just as its 256-dimensional illustration in Fig. 5.

III. Learning the Filter Bank

A. Algorithm

In the geometric perspective of *MOC*, the filters can be seen as hyperplanes that separate local patches (Fig. **??**(b)(c)(d)) apart. Intuitively, the local patch clusters apparently should not be separated by the hyperplanes. Thus we directly penalty the angles between the patches and the hyperplanes. For a given filter f_i, the optimal function is:

$$\max \frac{1}{N}\sum_{j=1}^{N} \arcsin \left| \frac{\mathbf{f}_i^T \hat{\mathbf{x}}_j}{\|\hat{\mathbf{f}}_i\| \|\hat{\mathbf{x}}_i\|} \right| \tag{3}$$

where,

$$\begin{aligned} \hat{\mathbf{f}}_i &= \text{Null}([f_0, f_1, \cdots, f_{i-1}])^T \mathbf{f}_i \\ \hat{\mathbf{x}}_j &= \text{Null}([f_0, f_1, \cdots, f_{j-1}])^T \mathbf{x}_j \end{aligned} \tag{4}$$

where f_i is the i-th vectorized filter, x_j is the j-th normalized image patch and $\text{Null}(\mathbf{A})$ denotes an orthonormal basis matrix for the null space of $\mathbf{A}$. The procedure of the algorithm is described as Algorithm 1.

Reshaping each column of F to square matrixes, the filters can be obtained (Fig. 3).

B. Analysis

*1) **A Homogeneous Histogram is Necessary**:* Since the direction of fingerprint curves cover all angles from 0 to π, we argue that in the *MOC* architecture, the segmentation criterion should guarantee that the given data distribution is partitioned as equally as possible. As the feature histograms show, some of the feature dimensions created by LBP and BSIF are always zero, which means the coding scheme is redundant. At the same time, a dimension with too high value may mix two or more discriminative components, leading to worse classification performance.

We simply use the entropy of feature histogram to quantize the homogeneousness of the features. For a given feature histogram $\mathbf{h}$ with dimension 2^d, the entropy is calculated as:

$$E(\mathbf{h}) = \sum_{i=0}^{2^d} -\mathbf{h}_i \log(\mathbf{h}_i + e) \tag{5}$$

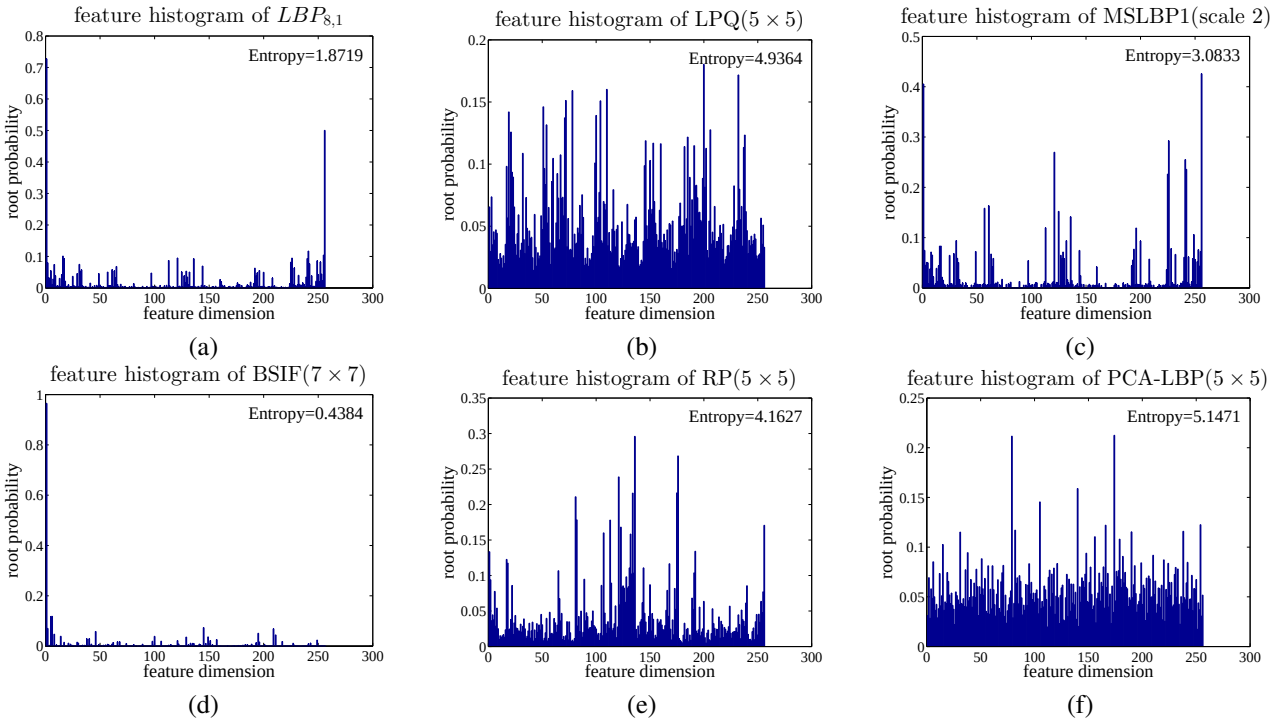

Fig. 5. The feature histogram by different algorithms. We plot the square root of the probabilities to get a better visual effect. Note that a "good" *MOC* algorithm ought to have a homogeneous histogram in theory, i.e. bigger entropy is better. (a) $LBP_{8,1}$ [23] with 3×3 filter size. (b) LPQ [24] with 5×5 filter size. (c) MSLBP1 [26] with 9×9 filter size. (d) BSIF [27] with 7×7 filter size. (e) Random filters with 5×5 filter size. (f) Our proposed method with 5×5 filter size.

Algorithm 1 The Proposed Learning Algorithm.

Require:

The set of normalized fingerprint image patches, X;
Initiate learning rate $\alpha_0 = 1$, line search scale $t = 1$;
Randomly initialised matrix F;
Initiate projection matrix $H = I$;

Ensure:

for $i = 1$ to d **do**
  $\hat{f}_i \leftarrow Hf_i$, $\hat{\mathbf{x}} \leftarrow Hx$.
  repeat
    Normalize $\hat{f}_i$ to ensure that $\|\hat{f}_i\| = 1$.
    Calculate the loss $L(\hat{f}_i; \hat{\mathbf{x}}) = \frac{1}{N}\sum_{j=1}^{N} \arcsin\left|\hat{f}_i^T \hat{x}_j\right|$ and the partial derivative $\frac{\partial L}{\partial \hat{f}_i} = \frac{1}{N}\sum_{j=1}^{N} \frac{sign(\hat{f}_i^T \hat{x}_j)}{\sqrt{1-(\hat{f}_i^T \hat{x}_j)^2}}\hat{x}_j$
    Line search for the learning rate α.
    Apply the partial derivative: $\hat{f}_i \leftarrow \hat{f}_i + \alpha \frac{\partial L}{\partial \hat{f}_i}$
  until $\|\frac{\partial L}{\partial \hat{f}_i}\| < 1e-8$
  $H \leftarrow Null(\hat{f}_i) \cdot H$
  $f_i \leftarrow H^T \hat{f}_i$
end for

where e is a small positive real number which is ultilized to avoid the operation of $\log(0)$. The more homogeneous the histogram $\mathbf{h}$ is, the bigger $E(\mathbf{h})$ will be (Fig. 5).

*2) **Our Generated Filters are Stable Regardless of Scale**:* As Fig. 6 illustrates, the filters of different scales are very similar, with only some changes of the order. The filters of higher scales are just enlarged ones of lower scales. This property reflects that our algorithm is scale-invariant, even though scale-invariant is not very necessary for fingerprint analyse as experiment shows (Fig. 8). However, it also indicates that when we connect the multi-scale features together, the information redundance is a severe problem. Dimension reduction is a indispensable part in our algorithm.

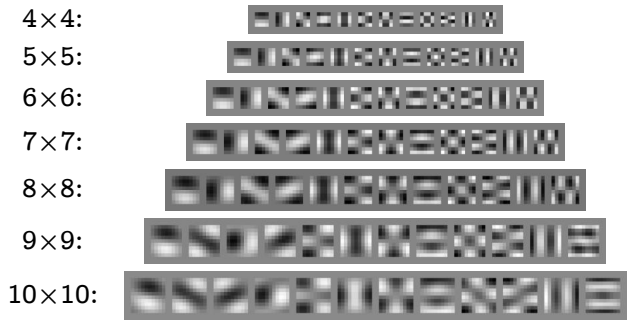

Fig. 6. The multi-scale filter pyramid generated by our learning algorithm. Note that the filters are stable regardless of the scale.

*3) **The Relationship Between the Filters from LPQ and Ours**:* It can be discovered that some of our learned filters are very similar to the ones generated by LPQ (Fig. 3). The feature histogram calculated by LPQ is as homogeneous as ours (Fig. 5). The reason why LPQ is suitable for fingerprint analysis is based on the assumption that the fingerprint images are just blurred fingerprint skeleton curves. The blurred black skeletons and the white background construct the two polarized

clusters in the joint distribution in Fig. **??**.(b). However, our algorithm can be easily extended to generate more filters while the filter number of LPQ is only 8. Since high dimensionality is one of the most important properties of our algorithm, the scalability is a very important property in *MOC* framework.

*4) **The relationship Between* MOC *and Bag-of-Words (*BoW*) Model:*** It can be noticed that the *MOC* is very similar to the *BoW* model [29], whose features are usually represented as the amounts of local features, such as image patches in this work, that locate around some given center points. However, the time complexity of extracting feature histogram used by *BoW* are too high for embedded systems. Suppose that the amount of the clusters is N, the time complexity of k-means or GMM at testing time is $\Theta(N)$, which means N times of convolution. In practice, we need at least hundred of clusters to get an acceptable performance. Meanwhile, the *MOC*, which is also a clustering algorithm, has a time complexity of $\Theta(log_2 N)$. In our method, we put the local patches into 4096 codes with only 12 times of convolution.

IV. High Dimensional Strategy

As we mentioned in Section III, most of the algorithms cannot provide homogeneous histograms. In the LBP framework, researchers raised up a merging strategy called "uniform" [23]. By combining the tiny components of the LBP feature together as a new one, they fix the histograms to endure more noises. Jia et al. [26] simply select the largest 1/4 patterns in the histogram to ignore the minutiae. None of the previous algorithms present a way to split the large components into small ones. Note that nearly all classifiers are able to find the discriminative linear combination of the features, while almost none of them could extract the latent components from only one dimension. Inspired by this property, we attempt to separate the feature space into more parts, i.e. to generate higher dimensional features.

High dimension strategy has been experimented to be effective in face recognition [30], [31]. It is noteworthy that most of the features used by Chen et al. [30], such as LBP [32], LE [33] and Gabor [34], are all *MOC* features. In this paper, we discover that high dimensional strategy is also critical to high performance of *MOC* in the fingerprint liveness detection task.

A. Dimension Increment

We extract higher dimensional features in the following two ways.

*1) **More Filters:*** Since the *MOC* framework's time complexity is only $\Theta(\log_2 N)$, it is very convenient to separate the space into more parts. In another words, by adding filters into the framework, the feature dimension will increase exponentially. In our learning algorithm, adding filters can be applied simply by changing the filter count d and training a few more iterations.

*2) **More Scales:*** Besides extracting high dimensional features, multiple scale is a widely-used technique to utilize the information from different resolutions. Compared to the handcrafted LBP and LPQ, our filters can change its size arbitrarily. So we can densely extract features from scale 3×3 to 10×10. Note that due to the zero-mean constraint (Equation 4), 3×3 patches only have 8 available principle components (filters). In other scales, we select 12 filters corresponding to the biggest 12 singular values to generate 4096 dimensional features.

B. Dimension Reduction

The over-split feature is apparently redundancy and noisy. Dimension reduction is necessary to filter the noise out and to learn a more compact feature. PCA is also competent for this job. The principle components that are corresponding to the highest correlations accommodate most of the information. Meanwhile, the noises have much lower correlations compared with the useful signals. They will be restrained by selecting the dominating directions.

Compressing the high dimensional combined feature directly is too expensive for a embedded system. Since features from different scales are calculated separately, we execute the PCA dimension reduction algorithm in each scale respectively. Then the lower dimensional features are connected and compressed again to eliminate the information redundancy of neighbour scales.

V. Experiment

A. Database

Our algorithm is compared with previous approaches on the four datasets from the Second International Fingerprint Liveness Detection Competition (LivDet2011 [20]). Each dataset contains 2000 live fingerprint images and 2000 fake ones acquired by the following electronic sensors: (i) Biometrika FX2000, (ii) Digital Persona, (iii) ItalData ET10 and (iv) Sagem MSO300. The fake fingerprints are made by materials of ecoflex , gelatine, latex, silicone and wood glue, for each material is used to generate 400 fake fingerprint. According to the LivDet2011 protocol, the datasets are divided into two parts equally, one for training and another for testing. All the models of various algorithms are trained in the training sets and the performances are obtained by applying the same models to the testing sets.

We do not choose the datasets of LivDet2013 [22] because most of the algorithms get very high performances on the first two datasets, Biometrika and Italdata. When the accuracy is generally above 95%, the performance of the models is mainly depended on the parameters and noises, regardless of the algorithms. On the Crossmatch dataset, nearly all the approaches, as well as ours, failed to give a satisfied result (no more than 50%). Because of the above reasons, we finally give up experimenting on the LivDet2013 database.

The performance of the approaches are estimated simply by the misclassification rate in the testing sets. In a real-world system, the misclassification risk of live or spoof fingerprints may be different. For instance, the users will feel bored when their real fingers are mistaken as spoof ones frequently. A developer may tend to raise up the misclassification risk of real fingers to improve the user experience. In contrary, a highly secret unit must increase the empirical risk of mistaking spoof fingerprints as real ones. For these reason, we also compare

the performance of different approaches by ROC curves. By fixing the false positive rate, developers can customize the system for different application scenarios.

To make our results more persuasive, we have implemented all the *MOC* algorithms mentioned above, such as LBP [28], LPQ [24], MSLBP1 [26] and BSIF [27]. Since the performance of the non-MOC algorithms are much worse than the MOC ones [26], [35], they are not taken into comparison.

B. Parameter Determination

We choose the support vector machine (SVM) with radial basis function kernel as our classifier. 10-fold cross validation is used to find the most satisfied dimension number of the final feature, and the parameters of the classifier. It is worthy to note that on all the datasets from LivDet2011, every 5 fingerprint images are collected from the same live or spoof finger. When we execute the 10-fold cross validation in usual way, the result is not reliable because it may be affected by the same direction map of the same finger. Instead of the totally random selection strategy, we divide the training sets into small groups of 5 fingerprint images generated from the same finger, and randomly select a subset of groups as test data.

When the accuracies of cross validation are the same with different parameters, we propose a simple method to determine which parameter is the best one. Note that if the confidence coefficient of a test sample in cross validation is close to 0, another sample that is similar to it will be possibly judged to another side. Suppose the confidence coefficient of a sample s is $T(s)$, then the decision variable D is calculated as:

$$D = \sum_{s} (0.1 - T(s))^2 \cdot \mathbf{1}\{T(s) < 0.1\} \tag{6}$$

where $\mathbf{1}\{\cdot\}$ represents a characteristic function when with $\mathbf{1}\{true\} = 1$, and $\mathbf{1}\{false\} = 0$.

Besides determination the dimension number of the final feature and the parameters of the classifier by cross validation, there are two hyper-parameters, filter count and preserved dimension number of every single scale, that should be set empirically.

*1) **Filter Number**:* We shows the accuracies of various dimensions in Fig. 7. It is illustrated that the performance increases as the dimension explosively grows. However, when the dimension increase to 2^{13}, the accuracies increase slightly or even decline. This is because there are only about 100,000 pixels in one fingerprint image. A 2^{13} dimensional feature means that only 10 codes contribute to each dimension in average. A weak noise with only a few outliers in one dimension will notably deteriorate the feature. Moreover, it is too huge to invoke a dimension reduction algorithm or a classifier on $2^{13} \sim 2^{15}$ dimensional features. Finally, we fix the filter number to 8 for scale 3×3 and 12 for scale 4×4 to 10×10.

*2) **Preserved Dimension Number of Single Scale**:* The effect of different number of dimensions after reduction in Biometrika dataset is illustrated in Fig. 8 as an example. It can be concluded that the potential dimension (threshold that the accuracy stop rising) increases with the scale, because features

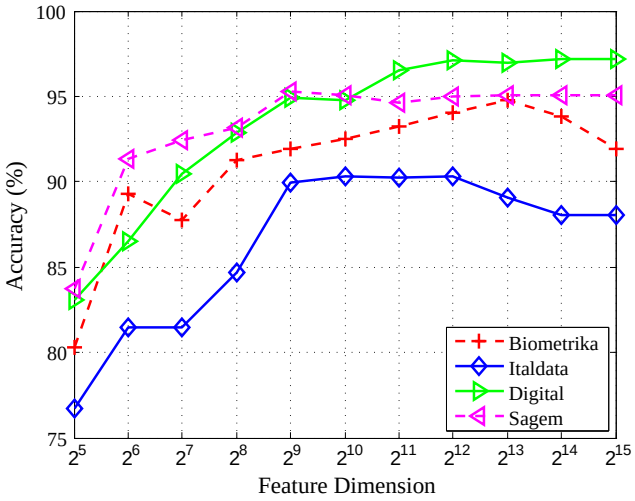

Fig. 7. Accuracy as a function of the feature's dimension in single scale. We only demonstrate the performance of 5×5 filters as an example.

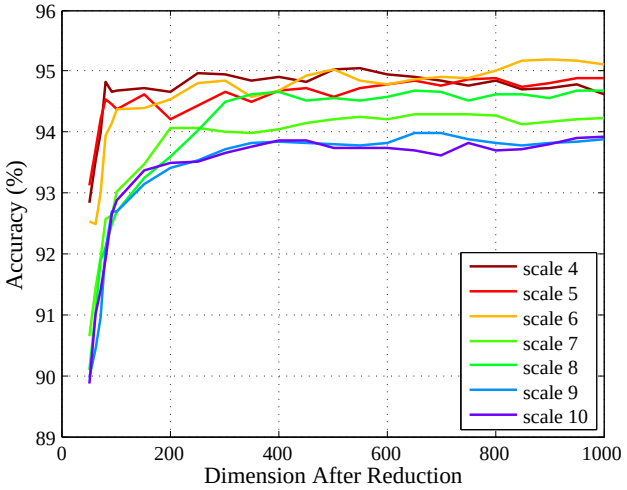

Fig. 8. The effect of the dimension reduction in various scales. We only demonstrate the results of Biometrika sensor as an example. Best view in color.

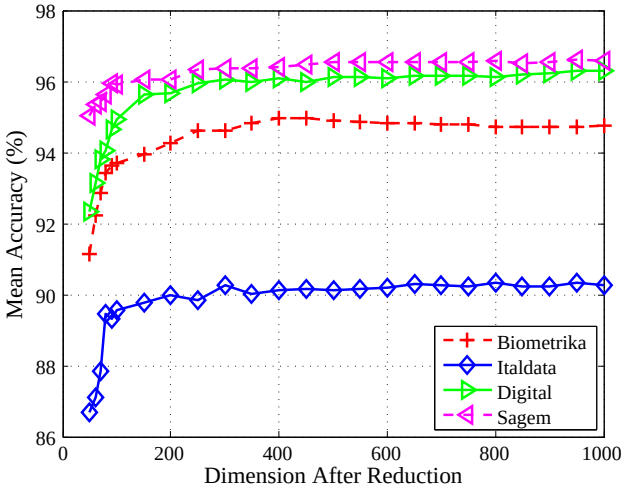

Fig. 9. The effect of the number of preserved dimension. The vertical coordinates are the average accuracy of all scales from 4 to 10.

extracted from high scale tend to contain more information. The average accuracies of all filter scales from 4×4 to 10×10 with different number of preserved dimension in the four datasets are illustrated in Fig. 9. According to Fig. 8 & 9, we fix the number of dimension after reduction in every single scale to 400 for all datasets.

C. Background Filtering

In a fingerprint image, fingerprint textures always do not cover all area of the image. Intuitively, the background should be wiped out, i.e., the features should be extracted in the region of fingerprint texture only. However, as we experimented, the accuracies decrease when we use a mask to filter the background out. We design an experiment to analysis the role of the background textures. The histogram features are computed on background only, fingerprint only and the whole image, respectively. The results are shown in Table I. Note that we only display the accuracies with scale 5×5 for rough demonstration.

TABLE I
EXPERIMENT RESULTS OF BACKGROUND FILTERING IN SCALE 5.

Region	Biometrika	Italdata	Digital	Sagem
All	5.95	10.15	2.9	5
No background	10.6	10.25	4.8	5
Background only	12.55	12.9	11.15	9.8
Soft background filtering	5.6	9.5	2.85	5

As the experimental results indicate, the performances of features extracted in background only are extremely beyond our expectation. The background implicitly accommodate some information that cannot be distinguished by naked eyes. When a real finger touches a optical fingerprint sensor, the effect of shadow tends to be stronger. The curves of knuckle may also be collected by the sensor (Fig. 10). Obviously, these minutiae should not be ignored.

Nonetheless, the blank regions in the background still should be erased out. We introduce a soft erasing method to avoid ignoring the useful information. Suppose that the i-th convolution result $\mathbf{N}_i = I * \mathbf{f}_i$, we define $\mathbf{N}_i(x, y)$ as *inactive* one if

$$abs(\mathbf{N}_i(x, y)) < \epsilon_i \tag{7}$$

where ϵ_i is a small positive number. If we guarantee that $||\mathbf{f}_i||_2 = 1$, ϵ_i can be set to 1, which means the threshold is 1 gray level away from the hyperplane $\mathbf{f}_i^T \mathbf{x} = 0$.

If more than half of the convolution results at position (x, y) are *inactive*, the arranged code $C_I(x, y)$ will be ignored in the histogram calculating step.

This technique only works with images that have large blank areas, such as some of the fingerprints collected by the Biometrika sensor and all fingerprints from Italdata sensor. When the fingerprints and background minutiae occupy most of the area in the images, the affect of it will be too little to be observed, such as fingerprints collected from Digital sensor and Sagem sensor.

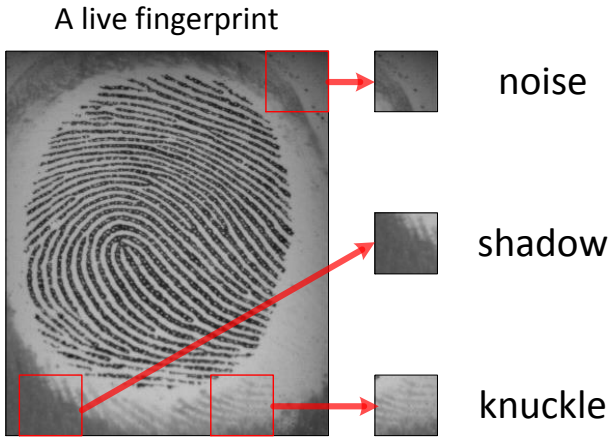

Fig. 10. A live fingerprint image with three types of background components labeled in the figure.

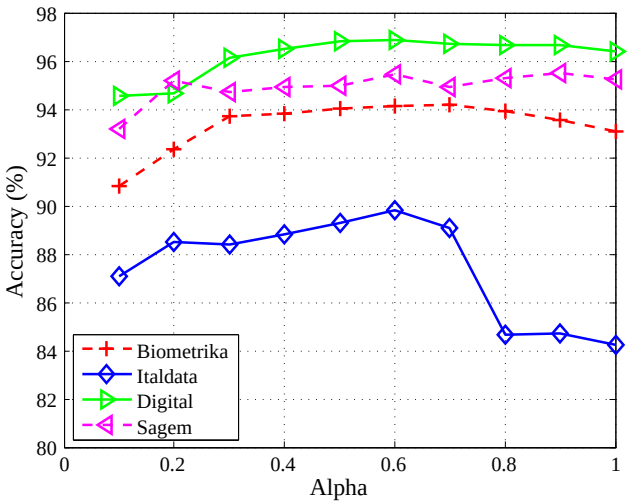

Fig. 11. The effect of α for normalization. We only demonstrate the performance of 5×5 filters as an example, because the time cost of cross validation for 4096 dimensional features is too expensive.

D. Normalization

As a histogram, the feature is normalized with $\ell 1$-norm. A simple technique may improve the performance significantly by powering the feature histogram $\mathbf{h}$ with a factor α:

$$\tilde{\mathbf{h}} = \mathbf{h}^{\alpha} \quad \alpha \in (0, 1) \tag{8}$$

In practice, the α can be obtained by cross-validation in the training set or just set to 0.6 which is widely adapted in all datasets (Fig. 11). The feature should be normalized with $\ell 1$-norm again after the α-normalization.

E. Performance of Random Filters

The most astonishing result is the performance of the random filters (TABLE II). By replacing the filters with random ones described in Section **??**, we have obtained accuracies no less than accuracies of LBP or LPQ. Furthermore, by combining 10 different random filter banks, the accuracies are very close or even beyond the state-of-the-art results got from

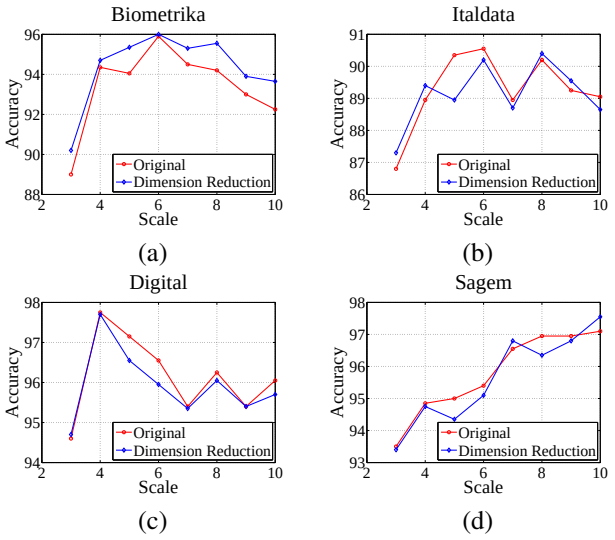

Fig. 12. Accuracy as a function of the filter window size (filter scale) in the four datasets. The performances of both original features and compressed ones are demonstrated here.

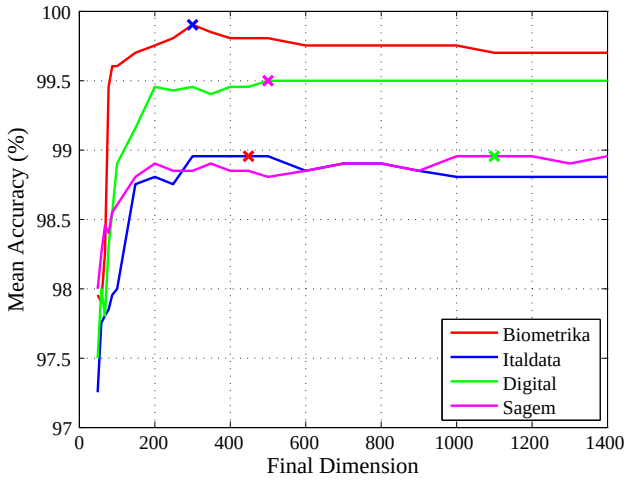

Fig. 13. The mean accuracy as a function of the final dimension in cross validation. Note that the best dimensions, which are determined by the cross validation accuracies and Equation (6), are marked by '×' in the figure. Best view in color.

BSIF and MSLBP[1]. These results reveal that it is the structure of the *MOC* rather than the well-designed filter banks that guarantees the high performance of *MOC* algorithms.

TABLE II
ACCURACY OF RANDOM PROJECTION AND BASELINES IN THE LIVDET 11 DATABASE

Algorithms	Biometrika	Italdata	Digital	Sagem
LBP [28]	89.05%	81.05%	89.45%	91.65%
LPQ [24]	85.35%	85.65%	88.05%	91.96%
MSLBP1 [26]	92.7%	85.2%	97.5%	94.7%
MSLBP2 [26]	89.4%	87.4%	93.3%	94.4%
BSIF [27]	93.2%	86.35%	96.5%	95.14%
RP minimum	89.5%	82.6%	93.1%	88.6%
RP maximum	92.6%	87.85%	95.15%	91.3%
RP average	91.32%	85.84%	94.23%	89.57%
RP combine	94.85%	89.1%	96.8%	93.6%

F. Performance of PCA Filters

Because of the high time and space cost of cross validation for high dimensional features, we empirically fix the α to 0.6, the number of preserved dimension to 400 for filter scale from 4×4 to 10×10 and 100 for filter scale 3×3. These hyper-parameters are not the best ones for each single scale, but they are passable choices for all scales in all datasets (Fig. 8, 9, 11).

*1) **Single Scale**:* The accuracies of various single scales of PCA filters is shown in Fig 12. As the figure illustrated, except for the low accuracy of scale 3 (due to its low dimension), there is no obvious regulation can be summed up with the scale changes, i.e., it is difficult to select a best scale for all the sensors.

*2) **Multiple Scales**:* The compressed features of all scales are combined together to form 2900 dimensional features. The features are further reduced to r dimensions, where r is determined by cross validation in the training sets, together with the parameters of the RBF-kernel SVM. We plot the effect of final dimension for all datasets in Fig. 13. The best dimensions calculated by Equation (6) are marked by '×' in the figure.

The misclassification rates of various *MOC* algorithms are listed in Table III, including the performance of the original 28928 dimensional features, compressed features, combined features extracted by random filters. Note that "DR" means dimension reduction in the table. The ROC curves of the four datasets are shown in Fig 14, respectively.

By combining all the features from various scales together, the final accuracy promotes a little bit except for the Digital dataset (Table III). This is mainly because the accuracies of different algorithms in Digital dataset are so high that the accuracies are sensitive to the noise in the image and the determination of the hyper-parameter. Due to the high dimension of the original features in our algorithm, it is difficult to apply a cross-validation algorithm to select the best parameters in every scale.

As is shown in the table and figure, our algorithm outperforms other algorithms under MOC framework in all the four datasets with a remarkable leap. However, when the system is subject to misclassifying live fingerprints to fake ones, such as only 1% false positive rate is acceptable, our algorithm is not always the best choice. For Digital Persona sensor or Sagem MSO300 sensor, when the false positive rate is set below 0.01, the true positive rate of our algorithm is lower than the one of BSIF [27] and MSLBP1 [26]. When the security level of a system is very high that the tolerance of spoof fingers is within a extremely low bound, our algorithm is a better choice for all the four sensors.

G. Further Experiments

Now that we have got accuracies of more than 90% on all the four sensors, with three of them beyond 95%. Does it mean that we can port the algorithm into a real verification system?

[1]Background filtering and normalization have been applied here.

TABLE III
COMPARISON OF ERROR IN THE LIVDET 2011 DATASETS

Algorithms	Biometrika	Italdata	Digital	Sagem	Mean	Std
PCA without DR	**2.45**	9.65	**2.65**	3.4	4.76	3.32
PCA with DR	3.5	**7.15**	2.6	**3**	**4.55**	2.73
RP combine	5.15	10.9	3.2	6.4	6.41	3.27
MSLBP1 [26]	7.3	14.8	**2.5**	5.3	7.48	5.27
MSLBP2 [26]	10.6	12.6	6.7	5.6	8.88	3.28
BSIF [27]	6.8	13.65	3.5	4.86	7.20	4.51
LBP [28]	11	19	10.6	8.35	12.24	4.66
LPQ [24]	14.7	14.4	12.0	8.0	12.27	3.10
LPQ+LBP [25]	10.4	13.2	8.0	5.3	9.23	3.37

Unfortunately, the high performance of the algorithm is based on the fact that we have already know the material and the manufacture technique of spoof fingerprint, which is unwarrantable in a real-world system. In fact, what we have been studying is a recognition problem, not liveness "detection". The fingerprint liveness detection is actually a one-class classification problem. We did a experiment on executing the one-class SVM algorithm on the live training dataset and test the performance in both live and spoof testing dataset. The classification rate is 57%, 55.6%, 62.75% and 69.25% respectively on the four datasets. Obviously, they are far from practical for a real-world application.

Mercifully, there are not too much materials competent for making spoof fingers. Since the main difficulty of one-class classification problem is the determination of the bound of the live and spoof fingerprints, we can use the spoof datasets which is already known to help confirming the bound. If we collect the materials and manufacture techniques as many as we can, the bound will be much clearer. Thanks to the organizers of the LivDet competition, fake fingers made by six different materials are utilized to collect fingerprint images (each dataset has five of them). We have done another experiment to determine the generalization performance of new materials. Similar with the experiment made in [26], we select four out of five materials in training set (1800 images) to train the model and test the accuracy rate of the remaining one in testing set (200 images). The result is shown in Table IV compared with the model trained with the whole training data (2000 images). As we could see in the table, the performances decrease rapidly except for only a few of them.

The algorithm is still far from solving the problem once and for all. As a Chinese proverb says, 'while the priest climbs a post, the devil climbs ten', we should not always follow the crackers' step. More methods, no matter algorithm-based, device-based or combined ones, should be explored to break this situation. Nonetheless, our proposed algorithm can still confront the already-known materials and techniques of making fake fingers. It would be practical if and only if the developers kept updating the model.

VI. CONCLUSION AND FUTURE WORK

In this paper, we introduced an simple but powerful data-driven algorithm to learn a filter bank which is satisfied with fingerprint image liveness classification. Besides, we presented a series of techniques, such as soft background filtering, normalization and the high dimension strategy, which are of benefit to the performance. Our algorithm outperforms the state-of-the-art approaches with a huge leap on all the four datasets in LivDet2011. Since our algorithm is purely software-based, it is very convenient to port it into the present fingerprint verification systems.

However, there are still many works to do. Firstly, since the liveness detection is a classification problem, a supervised learning or supervised fine-tuning algorithm may be a better choice. Secondly, a more powerful background noise filtering method may promote the performance further. Finally, our dimension reduction algorithm need to be improved. A single component should be a positive linear combination of a small subset of the high dimensional feature, while the components obtained by PCA always cover all the dimensions. An efficient sparse linear dimension reduction algorithm need to be exploited for the high dimensional data.

ACKNOWLEDGMENT

This research was supported by the National Natural Science Foundation of China (61201271, 61301269), the Fundamental Research Funds for the Central Universities (ZYGX2013J019, ZYGX2013J017), Sichuan Science and Technology Support Program (cooperated with the Chinese Academy of Sciences) (2012JZ001), and Science and Technology Support Program of Sichuan Province, China (2014GZX0009).

REFERENCES

[1] Nalini K. Ratha, Jonathan H. Connell, and Ruud M. Bolle, "Enhancing security and privacy in biometrics-based authentication systems", *IBM systems journal*, vol. 40, no. 3, pp. 614–634, 2001.
[2] Yogendra Narain Singh and Sanjay Kumar Singh, "Vitality detection from biometrics: state-of-the-art", in *IEEE World Congress on Information and Communication Technologies (WICT)*, 2011.
[3] Kristin A Nixon and Rowe et al., "Novel spectroscopy-based technology for biometric and liveness verification", in *Defense and Security*, 2004, pp. 287–295.
[4] Denis Baldisserra and Franco et al., "Fake fingerprint detection by odor analysis", in *Advances in Biometrics*, pp. 265–272. Springer, 2005.
[5] Lena Biel, Ola Pettersson, Lennart Philipson, and Peter Wide, "Ecg analysis: a new approach in human identification", *IEEE Transactions on Instrumentation and Measurement*, vol. 50, no. 3, pp. 808–812, 2001.

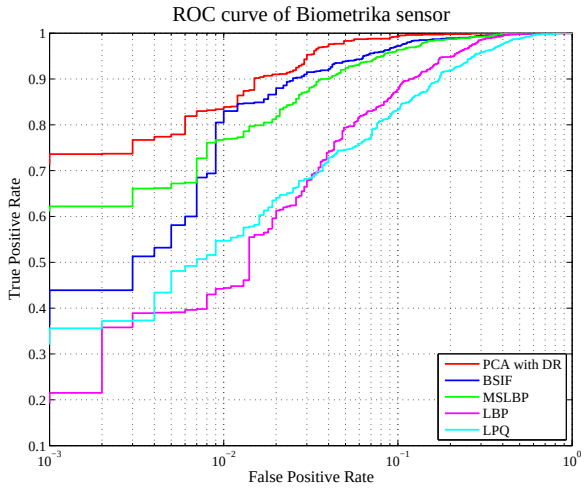

(a)ROC curves of Biometrika sensor

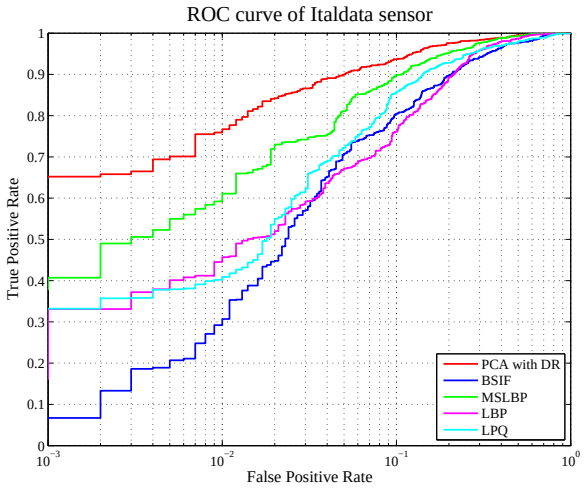

(b)ROC curves of ItalData sensor

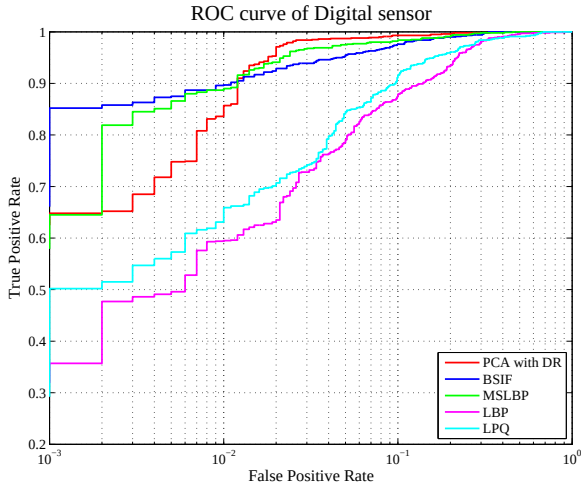

(c)ROC curves of Digital sensor

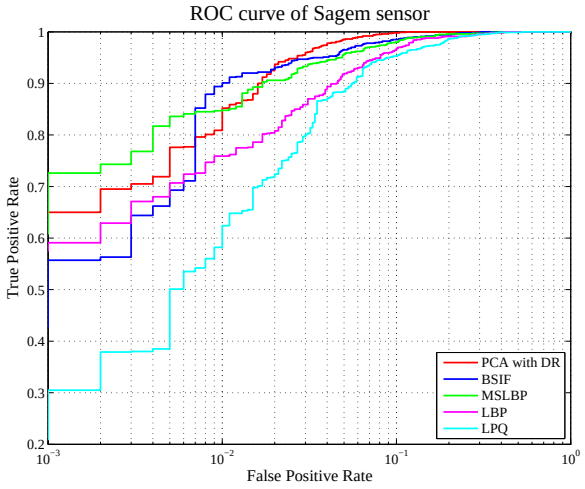

(d)ROC curves of Sagem sensor

Fig. 14. The ROC curves of the five *MOC* methods in four datasets.

[6] Kristin A Nixon and Robert K Rowe, "Multispectral fingerprint imaging for spoof detection", in *Defense and Security*. International Society for Optics and Photonics, 2005, pp. 214–225.

[7] Athos Antonelli, Raffaele Cappelli, Dario Maio, and Davide Maltoni, "Fake finger detection by skin distortion analysis", *IEEE Transactions on Information Forensics and Security*, vol. 1, no. 3, pp. 360–373, 2006.

[8] Jia Jia and Lianhong Cai, "Fake finger detection based on time-series fingerprint image analysis", in *Advanced Intelligent Computing Theories and Applications. With Aspects of Theoretical and Methodological Issues*, pp. 1140–1150. Springer, 2007.

[9] Yangyang Zhang, Jie Tian, Xinjian Chen, Xin Yang, and Peng Shi, "Fake finger detection based on thin-plate spline distortion model", in *Advances in Biometrics*, pp. 742–749. Springer, 2007.

[10] Jia Jia, Lianhong Cai, Kaifu Zhang, and Dawei Chen, "A new approach to fake finger detection based on skin elasticity analysis", in *Advances in Biometrics*, pp. 309–318. Springer, 2007.

[11] Pietro Coli, Gian Luca Marcialis, and Fabio Roli, "Power spectrum-based fingerprint vitality detection", in *IEEE Workshop on Automatic Identification Advanced Technologies*, 2007.

[12] Aditya S Abhyankar and Stephanie C Schuckers, "A wavelet-based approach to detecting liveness in fingerprint scanners", in *Defense and Security*. International Society for Optics and Photonics, 2004, pp. 278–286.

[13] Yiu Sang Moon, JS Chen, KC Chan, K So, and KC Woo, "Wavelet based fingerprint liveness detection", *Electronics Letters*, vol. 41, no. 20, pp. 1112–1113, 2005.

[14] Bozhao Tan and Stephanie Schuckers, "Liveness detection for fingerprint scanners based on the statistics of wavelet signal processing", in *IEEE Conference on Computer Vision and Pattern Recognition Workshop*, 2006.

[15] Shankar Bhausaheb Nikam and Suneeta Agarwal, "Fingerprint liveness detection using curvelet energy and co-occurrence signatures", in *International Conference on Computer Graphics, Imaging and Visualisation*. IEEE, 2008, pp. 217–222.

[16] Heeseung Choi, Raechoong Kang, Kyoungtaek Choi, Andrew Teoh Beng Jin, and Jaihie Kim, "Fake-fingerprint detection using multiple static features", *Optical Engineering*, vol. 48, no. 4, pp. 047202–047202, 2009.

[17] Reza Derakhshani, Stephanie AC Schuckers, Larry A Hornak, and Lawrence O'Gorman, "Determination of vitality from a non-invasive biomedical measurement for use in fingerprint scanners", *Pattern Recognition*, vol. 36, no. 2, pp. 383–396, 2003.

[18] Sujan TV Parthasaradhi, Reza Derakhshani, Lawrence A Hornak, and Stephanie AC Schuckers, "Time-series detection of perspiration as a liveness test in fingerprint devices", *IEEE Transactions on Systems, Man, and Cybernetics, Part C: Applications and Reviews*, vol. 35, no. 3, pp. 335–343, 2005.

[19] Bozhao Tan and Stephanie Schuckers, "Spoofing protection for fingerprint scanner by fusing ridge signal and valley noise", *Pattern Recognition*, vol. 43, no. 8, pp. 2845–2857, 2010.

[20] David Yambay, Luca Ghiani, Paolo Denti, Gian Luca Marcialis, Fabio Roli, and S Schuckers, "Livdet 2011‖fingerprint liveness detection competition 2011", in *International Conference on Biometrics*. IEEE, 2012, pp. 208–215.

[21] Gian Luca Marcialis, Aaron Lewicke, Bozhao Tan, Pietro Coli, Dominic Grimberg, Alberto Congiu, Alessandra Tidu, Fabio Roli, and Stephanie

TABLE IV
THE PERFORMANCE OF CROSS-MATERIAL CLASSIFICATION

	Biometrika	Italdata	Digital	Sagem	Sum
Ecoflex	**11/11**	38/23	*	*	49/34
Gelatine	32/14	37/26	114/0	99/28	282/68
Latex	22/7	12/2	74/27	32/0	140/36
Silgum	12/0	57/7	85/0	116/0	270/7
Woodglue	42/10	158/60	76/3	**0/0**	276/73
Playdoh	*	*	**0/3**	38/5	38/8
Sum	119/42	302/118	349/33	285/33	1055/226

Schuckers, "First international fingerprint liveness detection competitionłlivdet 2009", in *Image Analysis and Processing–ICIAP 2009*, pp. 12–23. Springer, 2009.

[22] Luca Ghiani, David Yambay, Valerio Mura, Simona Tocco, Gian Luca Marcialis, Fabio Roli, and Stephanie Schuckcrs, "Livdet 2013 fingerprint liveness detection competition 2013", in *Biometrics (ICB), 2013 International Conference on*. IEEE, 2013, pp. 1–6.

[23] Timo Ojala, Matti Pietikainen, and Topi Maenpaa, "Multiresolution gray-scale and rotation invariant texture classification with local binary patterns", *IEEE Transactions on Pattern Analysis and Machine Intelligence*, vol. 24, no. 7, pp. 971–987, 2002.

[24] Ville Ojansivu, Esa Rahtu, and Janne Heikkila, "Rotation invariant local phase quantization for blur insensitive texture analysis", in *International Conference on Pattern Recognition*. IEEE, 2008, pp. 1–4.

[25] Luca Ghiani, Gian Luca Marcialis, and Fabio Roli, "Fingerprint liveness detection by local phase quantization", in *International Conference on Pattern Recognition*. IEEE, 2012, pp. 537–540.

[26] Xiaofei Jia, Xin Yang, Kai Cao, Yali Zang, Ning Zhang, Ruwei Dai, Xinzhong Zhu, and Jie Tian, "Multi-scale local binary pattern with filters for spoof fingerprint detection", *Information Sciences*, , no. 0, pp. –, 2013.

[27] Luca Ghiani, Abdenour Hadid, Gian Luca Marcialis, and Fabio Roli, "Fingerprint liveness detection using binarized statistical image features", in *Biometrics: Theory, Applications and Systems (BTAS), 2013 IEEE Sixth International Conference on*. IEEE, 2013, pp. 1–6.

[28] Timo Ojala, Matti Pietikäinen, and David Harwood, "A comparative study of texture measures with classification based on featured distributions", *Pattern recognition*, vol. 29, no. 1, pp. 51–59, 1996.

[29] Li Liu and Paul Fieguth, "Texture classification from random features", *IEEE Transactions on Pattern Analysis and Machine Intelligence*, vol. 34, pp. 574 – 586, 2012.

[30] Dong Chen, Xudong Cao, Fang Wen, and Jian Sun, "Blessing of dimensionality: High-dimensional feature and its efficient compression for face verification", in *Computer Vision and Pattern Recognition (CVPR), 2013 IEEE Conference on*. IEEE, 2013, pp. 3025–3032.

[31] Oren Barkan, Jonathan Weill, Lior Wolf, and Hagai Aronowitz, "Fast high dimensional vector multiplication face recognition", in *Proc. IEEE Intl Conf. Computer vision*, 2013.

[32] Timo Ahonen, Abdenour Hadid, and Matti Pietikainen, "Face description with local binary patterns: Application to face recognition", *Pattern Analysis and Machine Intelligence, IEEE Transactions on*, vol. 28, no. 12, pp. 2037–2041, 2006.

[33] Zhimin Cao, Qi Yin, Xiaoou Tang, and Jian Sun, "Face recognition with learning-based descriptor", in *Computer Vision and Pattern Recognition (CVPR), 2010 IEEE Conference on*. IEEE, 2010, pp. 2707–2714.

[34] Chengjun Liu and Harry Wechsler, "Gabor feature based classification using the enhanced fisher linear discriminant model for face recognition", *Image processing, IEEE Transactions on*, vol. 11, no. 4, pp. 467–476, 2002.

[35] Luca Ghiani, Paolo Denti, and Gian Luca Marcialis, "Experimental results on fingerprint liveness detection", in *Articulated Motion and Deformable Objects*, pp. 210–218. Springer, 2012.

John Doe Biography text here.